An Analysis of the Critical Region of Multiparameter Equations of State

Ian H. Bell[1] · Eric W. Lemmon[1] · Allan H. Harvey[1]

Abstract

In this work, two classes of defects with multiparameter equations of state are investigated. In the first, it is shown that the critical point provided by equation of state developers often does not exactly meet the criticality conditions based on the first two density derivatives of the pressure being zero at the critical point. Based on the more accurate locations of the critical points given in the first part, the scaling of the densities along the binodal and spinodal in the critical region are investigated, and we find that the vast majority of equations have reasonable behavior but a few do not.

1 Introduction

Multiparameter Helmholtz energy equations of state (EOS) generally use many adjustable parameters [1] (more than 150 for the current international formulation for water) in order to fit the experimental data very accurately[2]. In so doing, they can also yield non-physical behavior if they are not appropriately constrained. The art of EOS development therefore rests on determining the correct set of constraints on EOS behavior that balances obtaining proper fluid behavior and accurately fitting the experimental data.

In the critical region along the saturation curves, one constraint that must be met is that the critical point given by the EOS developers meets the conditions to be a

---

✉ Ian H. Bell
ian.bell@nist.gov

1   Applied Chemicals and Materials Division, National Institute of Standards and Technology, 325 Broadway, Boulder, CO 80305, USA

⌖ Springer

critical point (described below). This work investigates how well this condition is actually met for multiparameter equations in use today.

This work is given in two parts. In the former, the ability of the EOS to represent the numerical critical point is investigated, and in the latter, critical region scaling applied to the orthobaric (saturated liquid and vapor) densities is investigated.

2 Methodology

The `teqp` open-source library [3] was used for all EOS evaluations. It is a new C++ library based on the use of automatic differentiation, allowing for very computationally efficient and maintainable implementations of Helmholtz-energy-explicit EOS of different kinds. The library includes implementation of cubic EOS, some SAFT models, as well as the multi-fluid model used in NIST REFPROP[4], Cool-Prop [5], and TREND [6].

The .FLD files that are included with REFPROP 10.0 were converted to the required input format of `teqp` with the code from the https://github.com/ianhbell/REFPROP-interop repository, and `teqp` was used for all calculations because it includes computational routines not presently available in REFPROP and correctly implements the derivatives of the so-called non-analytic terms due to its use of automatic differentiation.

3 Numerical Critical Point

The definition of a vapor–liquid critical point for a pure fluid is a temperature–density pair satisfying $(\partial p/\partial \rho)_T = (\partial^2 p/\partial \rho^2)_T = 0$. These two non-linear equations can be iteratively solved with Newton's method given a user-specified starting point. In theory, the critical point given by the EOS developers should satisfy the conditions, ideally to all digits available in double-precision arithmetic, so to more than 14 digits. In practice, many equations of state do not exactly satisfy the criticality constraints when the published critical temperature and density are substituted into the criticality constraints. In some cases the differences are small but non-zero; in others the differences are problematically large. While a temperature difference between the critical point given by the EOS developers and the numerical critical point of 0.001 K might sound small, this discrepancy has significant effects that effectively amplify the difference. Some computational implementations use numerical critical points and others use the published critical point, and the discrepancies can cause complications for the algorithm and sometimes result in erroneous results that can be traced back to this defect.

An example where this problem causes practical problems is to solve for the saturation temperature given an orthobaric density. The iterative routines for this problem in both NIST REFPROP [4] and CoolProp [5] fail with regularity; part of the problem comes from the erroneous critical points (a significant additional contribution comes from the loss in numerical precision in derivatives in this region [7]). In the critical region, the derivative $|d\rho^\pi/dT|$ goes to infinity (there is a singularity); π

is a placeholder for the bulk phase. Thus, the region between the critical point and a temperature even 0.0001 K below the critical temperature corresponds to a small but non-trivial density range. It is important to resolve the critical temperature as closely as possible, leaving no part of the density range without a corresponding saturation temperature.

In order to find the numerical critical point (or, in a few erroneous cases, critical points), the `solve_pure_critical` routine of `teqp` was used. This numerical critical point is defined to be the state point where the first and second derivatives of pressure with respect to temperature of the EOS are zero. The routine needs a starting point, so a large matrix of starting points in the range $[0.9T_{crit}, 1.3T_{crit}] \times [0.5\rho_{crit}, 2\rho_{crit}]$ was generated around the published critical point. From each starting point, the `solve_pure_critical` routine ot `teqp` attempted to obtain the numerical critical point with Newton iterations. Each solution was checked that it was within the initial box (not guaranteed), whether the critical conditions were still satisfied, and whether points at densities just above and below the solution density along the isotherm yield $\partial p/\partial \rho|_T > 0$, the condition for phase stability.

For most EOS, this process yielded many solutions, but all within a narrow distribution of the mean, the deviations from the mean being caused by noise in the iterative solving procedure. If the standard deviations of all the obtained temperatures were within 10^{-8} times the mean and the standard deviation of the molar densities were within 10^{-8} times the mean, the points were considered to be the same solution, and a single critical point was obtained, as presented in Table S1 in the supplementary information (SI). In a second step, a clustering algorithm was used to see whether multiple clusters of critical point solutions could be found; if only one was obtained, that was also considered to be a single critical point. Those with multiple clusters (in the end, only nitrogen) are presented in Table S2 in the SI. The EOS for which the differences are present are tabulated in Table S3 in the SI. The deviations in temperature and density are shown in Fig. 1. Intriguingly, there is a strong correlation between errors in the two state variables, the reason for which is unclear.

The worst deviations are highlighted in Fig. 2. Each of the EOS, with the exception of two (DEE and R40) from Thol et el. [8], were published in the 1990s, and since then the tools used to develop EOS have improved. The problem of erroneous numerical critical points is important to be aware of when using EOS, but should not happen in any new EOS.

In the case of refrigerant R-134a [9], Tillner-Roth and Baehr used a reducing temperature of 374.18 K while reporting a critical temperature based on experimental values of 374.21 K. The numerical critical temperature of their equation of state is 374.211967...K. Although this does not mean that VLE calculations are impossible with this EOS between 374.18 K and 374.211967...K, the inconsistency between reducing and critical temperatures causes all manner of complications in the critical region and this approach should never be used in future EOS development efforts; only the numerical critical point should be used as the reducing temperature. For a few other EOS, the reducing densities are not the same as the critical densities given by the EOS developers.

For the case of nitrogen[10], multiple critical points can be found within the search box (a few other EOS also have spurious critical points inside the spinodals,
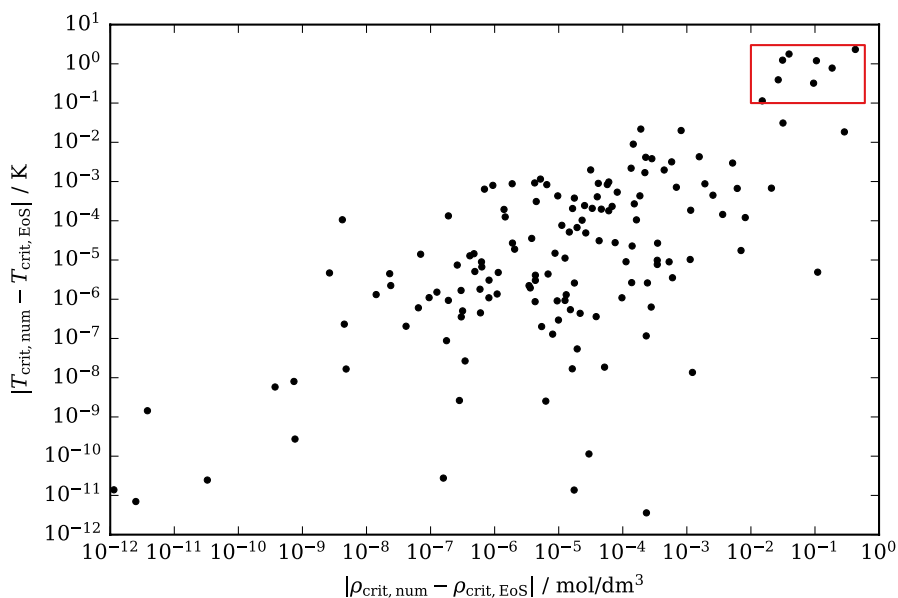
Fig. 1 Deviations between the mean obtained numerical critical point and the critical point given by the EOS developers for the default EOS in NIST REFPROP 10.0. The red box indicates the values highlighted in Fig. 2
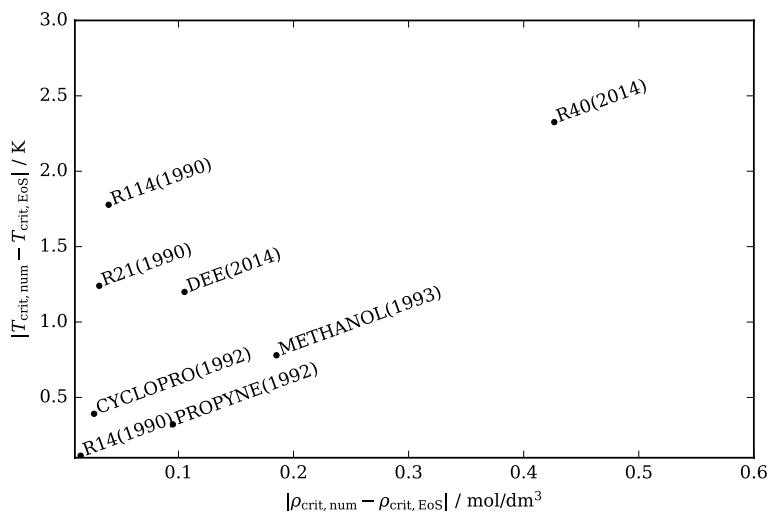
Fig. 2 Deviations between the mean obtained numerical critical point and the critical point given by the EOS developers for the default EOS in NIST REFPROP 10.0 for the EOS with the largest deviations. The year of publication of the EOS is indicated in the annotation of each point

when the spinodals are present). In the case of nitrogen, the spinodal does not cover the full saturation temperature range, and thus the additional critical point identified cannot be ruled out based on the location of the spinodal. The values are given in Table S3 in the SI.

In order to resolve the problems identified in this section, two solutions are available. The key cause of these problems is that the criticality conditions need to be enforced much more tightly throughout the EOS development. The criticality conditions are one of the only constraints that are known with great certainty from theory. Another source of problems is the rounding of EOS coefficients as the last step in the equation of state development; this rounding is to improve the aesthetics of the model coefficients, and to simplify manual entry when implementing the EOS, rather than having some statistical basis. Recent work [11] has shown that leaving two of the EOS coefficients unrounded can allow for a much more accurate numerical critical point, and that approach, if consistently applied, should fix the problem of incorrect numerical critical points going forward.

4 Critical Scaling

4.1 Theory

Critical scaling theory defines a scaling exponent β for the vapor–liquid coexistence curve that describes the asymptotic behavior of the equilibrium vapor and liquid densities as the critical point is approached:

$$\left(\rho' - \rho''\right) \sim \Theta^{\beta}, \tag{1}$$

where

$$\Theta = \left(\frac{T_{\text{crit,num}} - T}{T_{\text{crit,num}}}\right). \tag{2}$$

The critical exponent β is 0.5 within classical (mean-field) theories, so any analytic equation of state must give that result in the limit of the critical point. However, real fluids are not classical; they belong to the same universality class as the three-dimensional Ising model.[12–14] All systems in that universality class have the same set of critical exponents, differing from the mean-field values. The current best estimate for β for the Ising model (and therefore for real fluids) is approximately 0.3264.[15]

It has long been recognized that, at least in the presence of gravity, it is nearly impossible to get close enough to the critical point to observe the true asymptotic value of β, and that near-critical measurements of the coexistence curve typically produce an effective value of β near 0.35.[16, 17] It is empirically observed that this effective exponent continues to describe the coexistence curve fairly well even quite far below the critical point.

In order to analyze the behavior of equations of state, we define an "effective" value of β, β_{eff}, in a differential manner at each point on the coexistence curve; such analysis of effective exponents varying with distance from the critical point has proven useful in other contexts.[18–20] We construct separate effective exponents for the vapor and liquid branches of the coexistence curve, so that we have

$$\beta'_{\text{eff}} \equiv \frac{\text{d} \ln \left(\rho' - \rho_{\text{crit}} \right)}{\text{d} \ln(\Theta)} \tag{3}$$

$$\beta''_{\text{eff}} \equiv \frac{\text{d} \ln \left(\rho_{\text{crit}} - \rho'' \right)}{\text{d} \ln(\Theta)}. \tag{4}$$

At this point, we pause to consider what the behavior of β_{eff} "should" be for a multiparameter equation of state. For the real fluid, β_{eff} will approach the exact Ising value (~ 0.3264) at T_{crit}, taking values near 0.35 as one moves further down the coexistence curve. However, such behavior is impossible for the equations examined here, because their analytic nature means that β_{eff} will inevitably approach the mean-field value of 0.5 at the critical point. Therefore, the best that can be done by a classical equation of state is to retain a value of β_{eff} near 0.35 for most of the coexistence curve before transitioning to a (physically wrong) value of 0.5 at the critical point. If that transition to 0.5 is sufficiently close to the critical temperature, the wrong limiting exponent will not matter for practical calculations.

The other aspect of the behavior of β_{eff} that should be examined is its smoothness. If β_{eff} has significant oscillations away from the critical point, or swings above 0.5 or below 0.3 before transitioning to the critical value of 0.5, that is unphysical behavior that should be avoided.

It is very important to note that the numerical critical point obtained in the previous section of this paper should always be used in this analysis, otherwise spurious asymptotic limits on approaching the "critical point" may be obtained if the numerical critical point is not used and the EOS has a different numerical critical point than the given one.

As is clear from (3) and (4), when plotting $\ln(\Delta\rho^\pi)$ as a function of $\ln(\Theta)$, π indicating a placeholder for a phase, the slope is β^π_{eff}. The value of β^π_{eff} can be obtained for a given successful phase equilibrium iterative calculation (which yields ρ' and ρ'' for a given value of T) from

$$\beta^\pi_{\text{eff}} \equiv \frac{\text{d} \ln(\Delta\rho^\pi)}{\text{d} \ln(\Theta)} = \frac{\Theta}{\Delta\rho^\pi} \frac{\text{d}\Delta\rho^\pi}{\text{d}\Theta} = \frac{\Theta}{\Delta\rho^\pi} \frac{\dfrac{\text{d}\Delta\rho^\pi}{\text{d}T}}{\dfrac{\text{d}\Theta}{\text{d}T}}, \tag{5}$$

where $\text{d}\Delta\rho'/\text{d}T = \text{d}\rho'/\text{d}T$, $\text{d}\Delta\rho''/\text{d}T = -\text{d}\rho''/\text{d}T$, and $\text{d}\Theta/\text{d}T = -1/T_{\text{crit,num}}$.

The derivatives $\text{d}\rho'/\text{d}T$ and $\text{d}\rho''/\text{d}T$ can be obtained from exact derivatives of the EOS. The temperature derivative of the vapor pressure $\text{d}p_\sigma/\text{d}T$ is given by the Clapeyron relationship

$$\frac{\mathrm{d}p_\sigma}{\mathrm{d}T} = \frac{\Delta h}{T \Delta v}, \tag{6}$$

where h is the enthalpy and v is the specific volume, which was added to `teqp` version 0.14.3 as the function `dpsatdT_pure` and can be expressed in terms of residual properties only. The complete derivative comes from (see Ref. [21])

$$\frac{\mathrm{d}\rho^\pi}{\mathrm{d}T} = \left(\frac{\partial \rho}{\partial p}\right)_T \left(\frac{\mathrm{d}p_\sigma}{\mathrm{d}T} - \left(\frac{\partial p}{\partial T}\right)_\rho\right), \tag{7}$$

where the partial derivatives are evaluated for the bulk phase for each derivative and the vapor pressure derivative is the same for both phases.

4.2 Results for EOS

To assess the behavior of the orthobaric scaling exponents, VLE data were obtained in the near-vicinity of the critical point with the default EOS used in NIST REF-PROP indicated in Table S1 in the SI.

In order to generate VLE data in the critical region, calculations were started at $\Theta = 0.3$, and the normal ancillary equations were used to initialize the VLE calculations carried out with the `pure_VLE_T` function of `teqp`. The value of T was incremented by a small amount that decreased while approaching the critical point (the new temperature was calculated from $0.99T + (1 - 0.99) \times T_{\mathrm{crit}}$). The calculated values of $\mathrm{d}\rho'/\mathrm{d}T$ and $\mathrm{d}\rho''/\mathrm{d}T$ were multiplied by the step size ΔT to obtain the increment in the orthobaric densities, which was followed by a polishing step to meet the VLE conditions. This integration plus polishing method is the same successfully used in modern phase equilibrium tracing approaches for mixtures [22–25]. This process continued until the equilibrium saturated liquid and vapor densities differed by less than a part in 10^6, the VLE solution failed, or 10000 steps were taken. There is significant noise in the obtained results in the very near vicinity of the critical
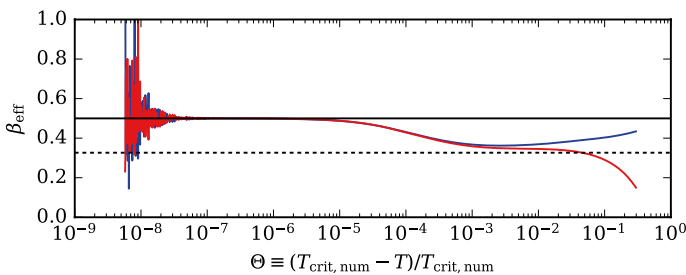
Fig. 3 The EOS for argon [27] demonstrating generally well-behaved asymptotic behavior in the near-critical region. The solid horizontal line for β_{eff} is the value 0.5, and the dashed horizontal line is the 3D Ising value. The liquid phase is in blue and the vapor phase is in red (Color figure online)
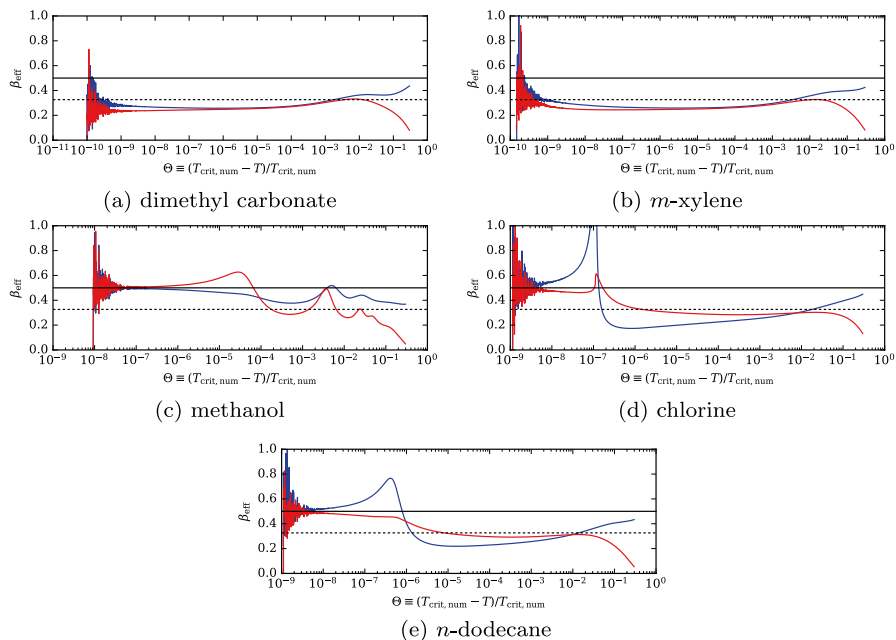
Fig. 4 Values of β_{eff} for each phase for selected equations of state demonstrating unusual (and incorrect in the last 3 cases) orthobaric density scaling. Further discussion of the plot formatting is in Fig. 3

point caused by the numerical difficulties in this region; to better resolve this region, extended precision numerical calculations are required [7, 26].

An example for what we believe to be a properly asymptotic EOS is shown in Fig. 3. The orthobaric density differences follow approximately a power-law relationship with the reduced temperature difference (identified by the value of β_{eff} approaching a constant value of 0.5) as the value of 0.5 is approached from below.

The argon-like behavior with β_{eff} smoothly approaching 0.5 for $\Theta < 10^{-3}$ does not always occur; some examples are shown in Fig. 4. In the first family of EOS (dimethyl carbonate and m-xylene), β_{eff} appears to approach a lower value instead of 0.5. This is not necessarily a flaw; β_{eff} would approach 0.5 if we could solve for vapor–liquid equilibrium closer to T_{crit}, which would require extended precision calculations. In the second family (methanol, chlorine, and n-dodecane), there are spurious wiggles in the curves, indicating defective behavior of the EOS.

The last two EOS to discuss are those of water [2] and carbon dioxide [28] (see Fig. 5). These EOS have special terms that make the critical region rather different than those of other EOS. However, because the Helmholtz energy can still be represented by a Taylor expansion at the critical point, the classical exponents should still be obtained. The EOS for water ([2]) does have an asymptotic behavior that is similar to argon, even if the precise shape of the

(a) water

(b) CO_2
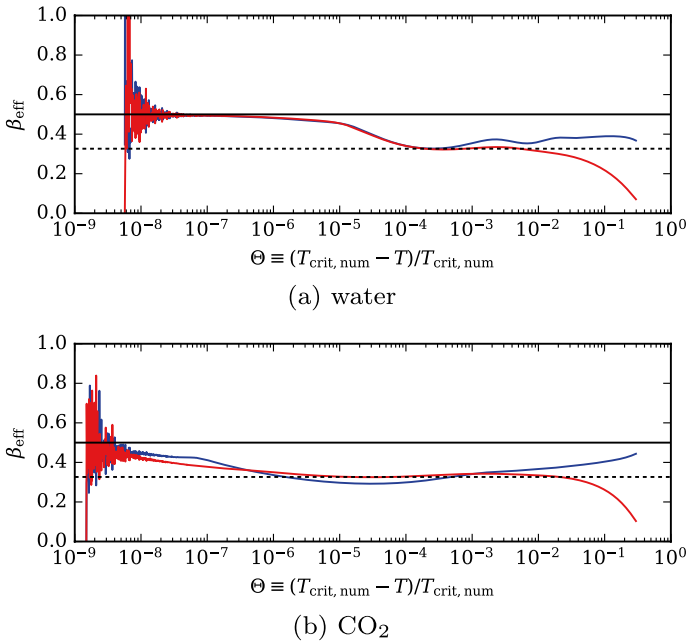
Fig. 5 Values of β_{eff} for each phase for water [2] and CO_2 [28]. Further discussion of the plot formatting is in Fig. 3

curves is a bit unlike that of argon. The curve for CO_2 eventually gets close to a value of β_{eff} near 0.5, but does not approach this value as quickly as argon. Note that this analysis cannot be carried out in NIST REFPROP because the higher density derivatives of the special terms have not been implemented.

5 Spinodals

Although the binodal is the curve for which scaling *must* apply, a similar approach can be applied to the spinodal in order to test the qualitative behavior of the equation of state. For a pure fluid, the definition for a point along the spinodal is a temperature, density pair that yields $(\partial p/\partial \rho)_T = 0$. This condition defines a curve in the temperature–density plane, with the critical point being the "top" of the spinodal. To build the locus, in the first calculation, the spinodal density on each side is obtained by starting from the ancillary equation provided with the EOS at a low enough temperature that convergence to the correct spinodal densities can be practically ensured. For subsequent temperatures, the previous spinodal density is used as a starting condition for the iteration for the temperature shifted away just slightly. In this way, the solver can reliably follow the spinodal to a point that is very close to the critical point. There are a few odd cases where the spinodals for the EOS stop abruptly and reappear in a new location. These generally occur with the high-accuracy equations developed between about 1990 and 2000 that were fitted with

linear methods and use high exponents for the temperature and/or density terms in the equations. Modern equations of state no longer suffer from this issue, having been developed with non-linear methods that allow for small exponents.

While we have not found a clear answer in the literature, we believe that a multiparameter EOS should also exhibit the classical limiting value of $\beta = 0.5$ for the scaling with temperature of the spinodal densities as they approach the critical point.

In order to calculate the density derivative along the spinodal, we first present a similar derivative for homogenous thermodynamic state points

$$\left(\frac{\partial \rho}{\partial T}\right)_p = -\frac{\left(\frac{\partial p}{\partial T}\right)_\rho}{\left(\frac{\partial p}{\partial \rho}\right)_T} \tag{8}$$

which is the familiar partial derivative of density with respect to temperature at constant pressure [21]. On the right-hand side, the quantity held constant (p in this case) appears twice in the derivatives. Similarly, the density derivative with respect to temperature along the spinodal (with subscript spin) is obtained from

$$\left(\frac{\partial \rho^\pi}{\partial T}\right)_{\text{spin}} = \left(\frac{\partial \rho^\pi}{\partial T}\right)_{(\partial p/\partial \rho)_T} = -\frac{\left(\frac{\partial^2 p}{\partial T \partial \rho}\right)}{\left(\frac{\partial^2 p}{\partial \rho^2}\right)} \tag{9}$$

so the mapping to the prior equation is a replacement of the quantity held constant ($(\partial p/\partial \rho)_T$, with a value of zero). With the definition from (5), an analogous quantity can be defined, where all densities refer to the densities along the spinodal rather than along the binodal.

It is not yet clear from a theoretical standpoint what the correct shape of the curve should be. Two spinodal curves are shown in Fig. 6. The general behavior for well-behaved EOS appears to be that the value of β_{eff} should smoothly approach 0.5 as the critical point is approached for both the metastable liquid and vapor phases. It is guaranteed that $(\partial^2 p/\partial \rho^2)_T$ will go to zero at the critical point (this is one of the critical point criteria), and $\partial^2 p/\partial T \partial \rho$ approaches a finite value at the critical point. The balance of the rates at which $\Theta/(\text{d}\Theta/\text{d}T) = T - T_{\text{crit}}$ and $(\text{d}\Delta\rho^\pi/\text{d}T)/\Delta\rho^\pi$ go to zero ultimately determine the limiting value of $\beta_{\text{eff, spin}}$ at the critical point.

6 Conclusion

It is shown that many EOS do not exactly meet the criticality constraints of $(\partial p/\partial \rho)_T = (\partial^2 p/\partial \rho^2)_T = 0$ at the critical point given by the EOS authors. This problem should not happen in any new multiparameter EOS due to the new technique of leaving two coefficients unrounded to enforce the criticality conditions [11].

(a) R-32
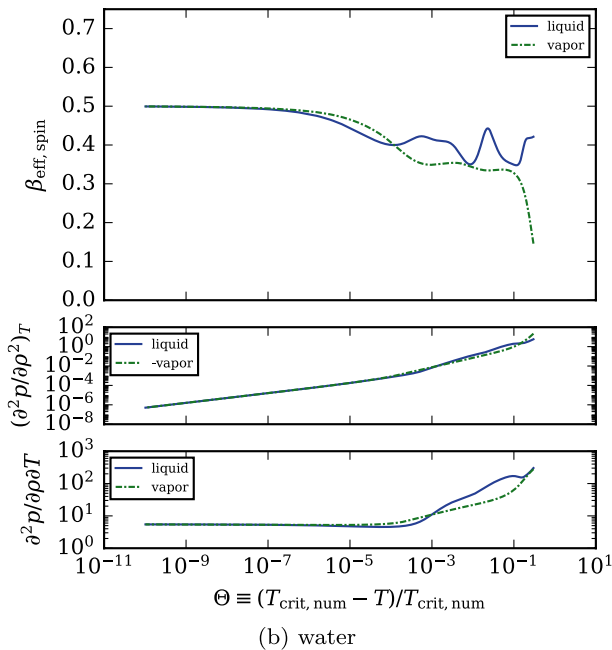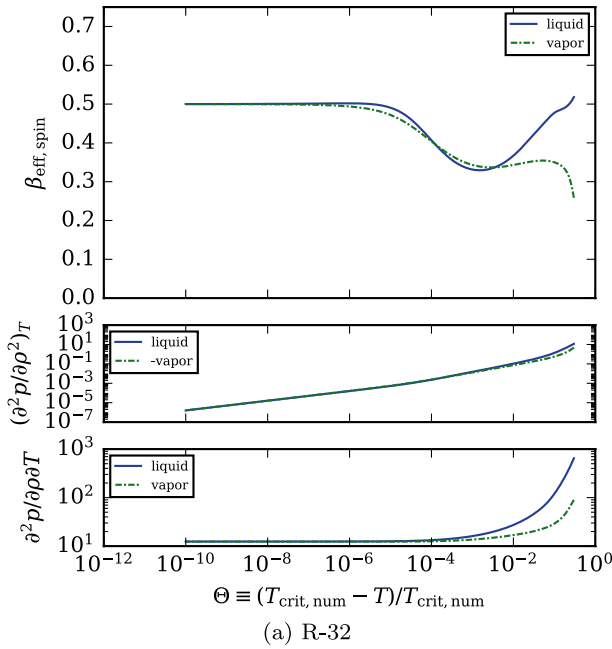
(b) water

Fig. 6 Values of $\beta_{\text{eff, spin}}$ and pressure derivatives for the spinodals for each phase for R-32 and water. Note the vapor phase has the sign of its $(\partial^2 p/\partial \rho^2)_T$ reversed for plotting purposes

This work also highlights that the effective scaling exponents for the orthobaric densities are important parameters to consider. It is to our knowledge the first time that these quantities have been considered in EOS development and they suggest the basis for a new set of EOS constraints in the critical region. An analysis of the orthobaric density scaling criterion along the spinodal yields preliminary insights about how the EOS should be constrained, even if the theory has not yet been developed on this point.

Data Availability In order to ensure reproducibility of our results, the supplementary information includes: A table of all the numerical critical points obtained; The orthobaric and spinodal scaling curves for all EOS in REFPROP 10.0. The corresponding author can be contacted for a copy of the scripts used to generate the figures

Declarations

Conflict of interest None

Ethical Approval Not applicable

References

1. R. Span, *Multiparameter Equations of State—An Accurate Source of Thermodynamic Property Data* (Springer, Berlin, 2000)
2. W. Wagner, A. Pruß, J. Phys. Chem. Ref. Data **31**, 387 (2002). https://doi.org/10.1063/1.1461829
3. I.H. Bell, U.K. Deiters, A.M.M. Leal, Ind. Eng. Chem. Res. **61**(17), 6010 (2022). https://doi.org/10.1021/acs.iecr.2c00237
4. E.W. Lemmon, I.H. Bell, M.L. Huber, M.O. McLinden. NIST Standard Reference Database 23: Reference Fluid Thermodynamic and Transport Properties-REFPROP, Version 10.0, National Institute of Standards and Technology. http://www.nist.gov/srd/nist23.cfm (2018). https://doi.org/10.18434/T4/1502528
5. I.H. Bell, J. Wronski, S. Quoilin, V. Lemort, Ind. Eng. Chem. Res. **53**(6), 2498 (2014). https://doi.org/10.1021/ie4033999
6. R. Span, R. Beckmüller, S. Hielscher, A. Jäger, E. Mickoleit, T. Neumann, S. Pohl, B. Semrau, M. Thol. TREND. Thermodynamic Reference and Engineering Data 5.0 (2020)
7. I.H. Bell, U.K. Deiters, Ind. Eng. Chem. Res. **60**(27), 9983 (2021). https://doi.org/10.1021/acs.iecr.1c00847
8. M. Thol, L. Piazza, R. Span, Int. J. Thermophys. **35**(5), 783 (2014). https://doi.org/10.1007/s10765-014-1633-1
9. R. Tillner-Roth, H.D. Baehr, J. Phys. Chem. Ref. Data **23**, 657 (1994). https://doi.org/10.1063/1.555958
10. R. Span, E.W. Lemmon, R.T. Jacobsen, W. Wagner, A. Yokozeki, J. Phys. Chem. Ref. Data **29**, 1361 (2000). https://doi.org/10.1063/1.1349047

11. E.W. Lemmon, R. Akasaka, Int. J. Thermophys. **43**(8), 19 (2022). https://doi.org/10.1007/s10765-022-03015-y
12. S.C. Greer, M.R. Moldover, Annu. Rev. Phys. Chem. **32**, 233 (1981). https://doi.org/10.1146/annurev.pc.32.100181.001313
13. M. Ley-Koo, M.S. Green, Phys. Rev. A **23**, 2650 (1981). https://doi.org/10.1103/PhysRevA.23.2650
14. M.E. Fisher, Rev. Mod. Phys. **70**, 653 (1998). https://doi.org/10.1103/RevModPhys.70.653
15. F. Kos, D. Poland, D. Simmons-Duffin, A. Vichi, J. High Energy Phys. **2016**, 36 (2016). https://doi.org/10.1007/JHEP08(2016)036
16. J.M.H. Levelt Sengers, J. Straub, M. Vicentini-Missoni, J. Chem. Phys. **54**(12), 5034 (1971). https://doi.org/10.1063/1.1674794
17. J.M.H. Levelt Sengers, W.L. Greer, J.V. Sengers, J. Phys. Chem. Ref. Data **5**(1), 1 (1976). https://doi.org/10.1063/1.555529
18. K.S. Pitzer, J.C. Tanger IV., Chem. Phys. Lett. **156**(4), 418 (1989). https://doi.org/10.1016/0009-2614(89)87120-9
19. M.A. Anisimov, S.B. Kiselev, J.V. Sengers, S. Tang, Physica A **188**(4), 487 (1992). https://doi.org/10.1016/0378-4371(92)90329-O
20. M.A. Anisimov, A.A. Povodyrev, V.D. Kulikov, J.V. Sengers, Phys. Rev. Lett. **75**, 3146 (1995). https://doi.org/10.1103/PhysRevLett.75.3146
21. M. Thorade, A. Saadat, Environ. Earth Sci. **70**, 3497 (2013). https://doi.org/10.1007/s12665-013-2394-z
22. I.H. Bell, U.K. Deiters, AIChE J. **64**, 2745 (2018). https://doi.org/10.1002/aic.16074
23. U.K. Deiters, Fluid Phase Equilib. **447**, 72 (2017). https://doi.org/10.1016/j.fluid.2017.03.022
24. I.H. Bell, U.K. Deiters, A. Jäger, Ind. Eng. Chem. Res. **61**(6), 2592 (2022). https://doi.org/10.1021/acs.iecr.1c04703
25. U.K. Deiters, I.H. Bell, Ind. Eng. Chem. Res. **59**(42), 19062 (2020). https://doi.org/10.1021/acs.iecr.0c03667
26. I.H. Bell, U.K. Deiters, Ind. Eng. Chem. Res. **62**(4), 1958 (2023). https://doi.org/10.1021/acs.iecr.2c02916
27. C. Tegeler, R. Span, W. Wagner, J. Phys. Chem. Ref. Data **28**, 779 (1999). https://doi.org/10.1063/1.556037
28. R. Span, W. Wagner, J. Phys. Chem. Ref. Data **25**, 1509 (1996). https://doi.org/10.1063/1.555991